p-wave photodetachment in a static electric field

N. D. Gibson, B. J. Davies, and D. J. Larson
Department of Physics, University of Virginia, Charlottesville, Virginia 22901
(Received 10 December 1992)

Photodetachment from negative ions initially bound in s states has been studied in a static electric field. A 10-keV ion beam was sent through a region with fields of up to 1.5 kV/cm applied parallel to the beam direction. A pulsed dye-laser beam, perpendicular to the ion beam, photodetached the ions. The relative cross sections were measured by detecting the resulting fast neutral atoms with a gated channeltron detector. Polarization-dependent electric-field oscillations were oberved on the p-wave detachment cross section of Au^- near the threshold at 18 620.2 cm^{-1}. A simple theory for calculating the oscillatory structure is presented. Good agreement is found between the data and the theory, for laser polarizations both parallel to and perpendicular to the static electric field.

PACS number(s): 32.80.Fb, 32.60.+i

I. INTRODUCTION

During the last decade, there has been much interest in the way an electric field modifies photodetachment cross sections. There have been a number of calculations [1–11] and at least four series of experiments investigating this effect [12–20]. There is qualitative agreement between theory and experiment. However, the experimental studies have not provided definitive tests of the theoretical work.

The first announced observation of the effects of an electric field on the photodetachment cross section was by Bryant *et al.* in 1987 [12]. They observed the effects of a motional electric field of about 1 MV/cm on photodetachment from a relativistic H^- beam. Further work by the same group was later reported for motional fields (Stewart *et al.* [13]), and subsequently for static fields in the 60–100-kV/cm range (Harris *et al.* [14]). Data from all three experiments were compared with the theory of Rau and Wong [6] and appeared to be in general agreement.

The first known recorded electric-field effects were oscillations on the Rb^- photodetachment cross section near the $5p_{1/2}$ excited-state threshold measured by Frey and co-workers [15,16]. However, these oscillations were not understood to be due to the approximately 1-V/cm electric field that was applied to extract the detached electrons until Greene and Rouze modeled the effect in 1988 [17]. Greene and Rouze point out that the periodicity of the oscillations agrees with the model, but that the amplitude of the oscillations is not quantitatively correct. This lack of agreement may be due to the complication of having more than one available detachment channel.

In 1990, Baruch and co-workers carried out s-wave photodetachment experiments from Cl^- and S^- in a 2.7-GHz microwave field, in part to test for the presence of a large ponderomotive shift in the photodetachment threshold [18,19]. Since the coherence time of the detachment (for example, the time between stochastic phase changes in the optical field, the time between collisions between the ions and background gases, etc., see Refs. [18,20]) was short compared to the period of the microwave field, this experiment did not show a ponderomotive shift. Instead, the results were found to be consistent with a simple model for photodetachment in a static electric field when time averaging of the field amplitude was taken into account. The time averaging reduces the expected oscillation amplitude by more than a factor of 2 and changes the phase of the oscillations. Some further averaging was introduced since the microwave field strength varied somewhat over the regions of data collection. The applied fields were about 3 kV/cm. The data seemed to be in reasonable agreement with the theory, but questions were raised by some possible discrepancies near threshold.

s-wave photodetachment in an electric field was studied in more detail by Gibson, Davies, and Larson [21]. Detachment from S^- and Cl^- was studied in static electric fields ranging from 500 to 1500 V/cm and was compared with theory. This work was the first study involving nonhydrogenic ions undergoing single channel photodetachment in a truly static field. Good agreement between data and theory was found for the phase and periodicity of the oscillations but the amplitude of the oscillations was found to be reduced to about 0.8 of the value obtained by the simplest theoretical model [19]. The discrepancies near threshold noted by Baruch *et al.* were not seen. The results of the s-wave work motivated the present work on p-wave detachment.

The two most obvious ways to observe p-wave detachment are to employ two-photon detachment processes from ions bound in p states, thereby allowing $\Delta l=0$, or to use single-photon detachment from ions initially bound in s states or d states. Since two-photon photodetachment rates are much smaller than single-photon detachment rates, and the thresholds of negative ions initially bound in d states are in a difficult wavelength range, we chose to investigate single-photo detachment from Au^- ions ($6s^2$).

Near threshold, the behavior of field-free photodetachment cross sections is described by the Wigner law [22]. The Wigner law states that the magnitude of the cross section is proportional to the energy above the photode-

tachment threshold raised to the $l+\frac{1}{2}$ power, where l is the angular momentum of the electron in its final state. Applying an electric field produces below-threshold detachment as well as oscillations on the cross section above the zero-field threshold and a nonzero cross section at this threshold. We will describe these effects using a simple model which treats the negative ion as an electron bound in a short-range potential and the detached electron as a free electron in a static field. This model is based upon the model previously used to describe s-wave detachment [21] and is closely related to previous works [3,6,8].

The physical mechanisms at work here are the same as for s-wave detachment. The electric field adds a sloping potential to the short-ranged ionic potential seen by the electron. Below the zero-field threshold, the now finite-width potential barrier on one side of the atom allows the bound electron to tunnel out. Above threshold, the part of the emerging electron's wave function that travels towards the higher potential region is reflected from the potential slope of the electric field. If the time to travel to the potential barrier and back is short compared to the coherence time of the detachment event, the reflected part of the electron wave packet will interfere with the part originally propagating down the potential hill. This interference produces oscillations on the cross section. In p-wave detachment, the amplitude of the oscillations is dependent on the orientation of the lobes of the continuum wave function, and is therefore dependent on the polarization of the detaching light.

The purpose of the experiments described here was to acquire definite p-wave data in a static field. The applied fields varied between 984 and 1476 V/cm. As in the microwave experiment and our previous s-wave work, we measure the ratio of the cross section with the electric field on to that with the field off. Measuring this ratio removes normalization errors between the field-on and field-off detachments and largely eliminates effects of the overall shape of the cross section. Since the ratio of field-on to field-off detachment can be measured to higher precision than the cross section, directly measuring the ratio provides a better test of the effects of an electric field. If we assume a known threshold, the only variable parameter in the calculation of the ratio is the strength of the electric field. Since the electric field's effects on p-wave detachment are polarization dependent, detachment was studied with the laser polarization both parallel to and perpendicular to the static electric field.

II. THEORETICAL DESCRIPTION

We can calculate the cross section for photodetachment from a negative ion using first-order time-dependent perturbation theory and the dipole approximation. From Fermi's "golden rule" we can get the following expression for the cross section:

$$\sigma=4\pi^2\alpha E_p\int d\zeta|\langle\Psi_f(\zeta)|\hat{\mathbf{e}}\cdot\mathbf{r}|\phi_i\rangle|^2\delta(E_i+E_p-E_f)\ , \quad (1)$$

where $\alpha=e^2/\hbar c$ is the fine-structure constant, ζ describes the scale in which the continuum final state is normalized, $\hat{\mathbf{e}}$ is the laser light's polarization vector, and E_i, E_f, and E_p are the initial-state, final-state, and photon energies. We need a representation for the initial-state and final-state wave functions to evaluate the cross section.

In this work we will consider photodetachment from ions that are initially bound in s orbitals. As there is no lower angular momentum state for the electron to enter, the $\Delta l=\pm1$ selection rule restricts us to p-wave detachment. As mentioned in the Introduction, there have already been a number of calculations of the electric-field effects on the cross section for p-wave photodetachment. To elucidate the essential features we will present a relatively simple derivation. The results of the calculation are not sensitive to the choice of the initial-state wave function. We choose to use a Gaussian function to represent the initial state. We use

$$|i\rangle=D_0\left[\frac{\beta}{\pi}\right]^{3/2}e^{-\beta x^2}e^{-\beta y^2}e^{-\beta z^2}\ , \quad (2)$$

where β is a size parameter and D_0 is an arbitrary constant. This state is normalized so that in the limit of an infinitely narrow Gaussian ($\beta\rightarrow\infty$), we get a δ function times D_0. Since the static field is small on the atomic scale (1 a.u.$=5.142\times10^9$ V/cm), we assume that the initial state is unaffected by the external field.

We solve the Schrödinger equation to find an expression for the final state in the static field. Since the negative ion potential is short ranged, we assume that there is no interaction between the departing electron and the neutral atom. The Schrödinger equation for the electron in the static field can be written as

$$\frac{-\hbar^2}{2m}\left[\frac{d^2}{dx^2}+\frac{d^2}{dy^2}\right]\Psi-\left[\frac{\hbar^2}{2m}\frac{d^2}{dz^2}+eFz\right]\Psi=\left[\frac{\hbar^2}{2m}[k_x^2+k_y^2]+\epsilon_z\right]\Psi\ , \quad (3)$$

where F is the strength of the static electric field, taken to be directed along the z axis, m is the mass of the electron, e is the charge on the proton, k_x and k_y are the wave vectors describing the motion in the x and y directions, and ϵ_z is the energy associated with the motion in the z direction. The solution to Eq. (3) is a product state which can be written as a plane wave in the two directions perpendicular to the electric field and as an Airy function in the direction of the field [23]. We can write this total wave function as

$$\Psi_{k_x,k_y,\epsilon_z}(x,y,z)=\frac{e^{ik_x x}}{\sqrt{\pi}}\frac{e^{ik_y y}}{\sqrt{\pi}}\left[\frac{4m^2}{e\hbar^4F}\right]^{1/6}\mathrm{Ai}(-\gamma)\ , \quad (4)$$

where $\mathrm{Ai}(-\gamma)$ is the Airy function and $\gamma=(z+\epsilon_z/eF)(2meF/\hbar^2)^{1/3}$. The constants occurring in Eq. (4) are chosen so that the wave function is k normalized in the x and y dimensions and ϵ normalized in the z dimension,

$$\int d^3r\,\Psi^*_{k_x k_y\epsilon_z}(x,y,z)\Psi_{\kappa_x\kappa_y\varepsilon_z}(x,y,z)=\delta(k_x-\kappa_x)\delta(k_y-\kappa_y)\delta(\epsilon_z-\varepsilon_z)\ . \quad (5)$$

The increasingly rapid oscillation of the Airy function as the value of the argument increases corresponds to the electron's kinetic energy increasing as it moves down the potential slope. The exponential decay of the Airy function for positive argument represents the wave function's penetration into the potential barrier of the field.

Similarly, for the field-free case, the final-state wave function is given by the solution to the Schrödinger equation for a free electron [Eq. (3) with $F=0$],

$$\Psi_{k_x,k_y,\epsilon_z}(x,y,z)=\frac{e^{ik_x x}}{\sqrt{\pi}}\frac{e^{ik_y y}}{\sqrt{\pi}}\left[\frac{m}{2\hbar^2\epsilon_z}\right]^{1/4}\frac{e^{ik_z z}}{\sqrt{\pi}}\ , \tag{6}$$

where the normalization is consistent with Eq. (5).

These solutions neglect the effects of the neutral core on the final state. This treatment is valid only near threshold where the wavelength of the final-state wave function is very large compared to the range of the initial state. Since the negative ion has a size of $(4-6)a_0$, we are constrained to the region where the electron wavelength $\lambda \gg 10a_0$ which gives $E \ll h^2/200ma_0^2 \approx 1$ eV. Since 1 eV ≈ 8000 cm^{-1}, and our data range does not exceed 50 cm^{-1} above threshold, this condition is well satisfied.

Since p-wave detachment is anisotropic, we would expect p-wave electric-field effects to be polarization dependent. For single-photon processes from ions initially bound in s states, the p-wave detachment lobes are aligned with the incoming light's polarization direction. We will first calculate an expression for the cross section with laser light polarized parallel to the electric field.

Using Eqs. (2) and (4), the matrix element can be written explicitly. Due to the symmetry of the x and y integrands, only the even part of the plane wave contributes, and the matrix element is given by

$$\langle f|\hat{\mathbf{e}}\cdot\mathbf{r}|i\rangle=\int\frac{\cos(k_x x)}{\sqrt{\pi}}\frac{\cos(k_y y)}{\sqrt{\pi}}\left[\frac{4m^2}{e\hbar^4F}\right]^{1/6}\mathrm{Ai}(-\gamma)\times\left[\frac{\beta}{\pi}\right]^{3/2}D_0 z e^{-\beta x^2}e^{-\beta y^2}e^{-\beta z^2}\times dx\,dy\,dz\ , \tag{7}$$

where the scalar product leaves only the z term, since the laser polarization is parallel to the electric field. We will make use of the following relation to perform the x and y integrations:

$$\int_{-\infty}^{\infty}e^{-a^2x^2}\cos(bx)\,dx=\frac{\sqrt{\pi}\,e^{-b^2/4a^2}}{a}\quad\text{for } a>0\ . \tag{8}$$

Equation (7) then simplifies to

$$\langle f|\hat{\mathbf{e}}\cdot\mathbf{r}|i\rangle=\frac{D_0}{\pi}\left[\frac{\beta}{\pi}\right]^{3/2}\left[\frac{\pi}{\beta}\right]e^{-k_x^2/4\beta}e^{-k_y^2/4\beta}\times\left[\frac{4m^2}{e\hbar^4F}\right]^{1/6}\int_{-\infty}^{\infty}\mathrm{Ai}(-\gamma)ze^{-\beta z^2}dz\ . \tag{9}$$

Now we can substitute Eq. (9) into Eq. (1) to find the cross section σ_F in the electric field.

$$\sigma_F=4\pi^2\alpha E_p\int\left[\frac{D_0}{\pi}\right]^2\left[\frac{\beta}{\pi}\right]e^{-k_x^2/2\beta}e^{-k_y^2/2\beta}\times\left[\frac{4m^2}{e\hbar^4F}\right]^{1/3}\left[\int_{-\infty}^{\infty}\mathrm{Ai}(-\gamma)ze^{-\beta z^2}dz\right]^2\times dk_x\,dk_y\,d\epsilon_z\,\delta(E_p-E_a-E)\ . \tag{10}$$

Since the laser polarization is parallel to the electric field, there is cylindrical symmetry and we can change our integration variables to ϵ_z and $E_\perp=(\hbar^2/2m)(k_x^2+k_y^2)$. Using the relationship $dk_x\,dk_y=k_\perp dk_\perp d\phi=2\pi(m/\hbar^2)dE_\perp$, the cross section is

$$\sigma_F=4\pi^2\alpha E_p\left[\frac{D_0}{\pi}\right]^2\left[\frac{\beta}{\pi}\right]\times\int d\epsilon_z\int e^{-mE_\perp/\beta\hbar^2}\left[\frac{4m^2}{e\hbar^4F}\right]^{1/3}\left[\frac{2\pi m}{\hbar^2}\right]\times\left[\int_{-\infty}^{\infty}\mathrm{Ai}(-\gamma)ze^{-\beta z^2}dz\right]^2dE_\perp\times\delta(E_p-E_a-E_\perp-\epsilon_z)\ . \tag{11}$$

Performing the integral over the δ function gives

$$\sigma_F=4\pi^2\alpha E_p\left[\frac{D_0}{\pi}\right]^2\left[\frac{\beta}{\pi}\right]\times\int_{-\infty}^{E_p-E_a}d\epsilon_z\left[\frac{4m^2}{e\hbar^4F}\right]^{1/3}e^{-m(E_p-E_a-\epsilon_z)/\beta\hbar^2}\times\left[\frac{2\pi m}{\hbar^2}\right]\left[\int_{-\infty}^{\infty}\mathrm{Ai}(-\gamma)ze^{-\beta z^2}dz\right]^2\ . \tag{12}$$

In order to account for electron tunneling at energies below the field-free threshold, the lower limit of the integral is negative infinity. Converting to atomic units ($m=\hbar=e=1$), the cross section for p-wave photodetachment in an electric field parallel to the incoming laser light's polarization direction is

$$\sigma_F=8\alpha E_p D_0^2\left[\frac{4}{F}\right]^{1/3}\beta\times\int_{-\infty}^{E_p-E_a}d\epsilon_z\,e^{-(E_p-E_a-\epsilon_z)/\beta}\times\left[\int_{-\infty}^{\infty}\mathrm{Ai}(-\gamma)ze^{-\beta z^2}dz\right]^2\ . \tag{13}$$

Equation (13) can be numerically integrated using an approximation for the z integral described below. The solid line in Fig. 1 shows this cross section in 1000- and 1500-V/cm electric fields.

We can calculate the zero-field cross section for p-wave detachment in a similar fashion. As before, only the even part of the x and y plane waves will contribute to the integrals. In addition, only the odd part of the z plane wave contributes. Considering only these parts, the free-electron wave function is given by

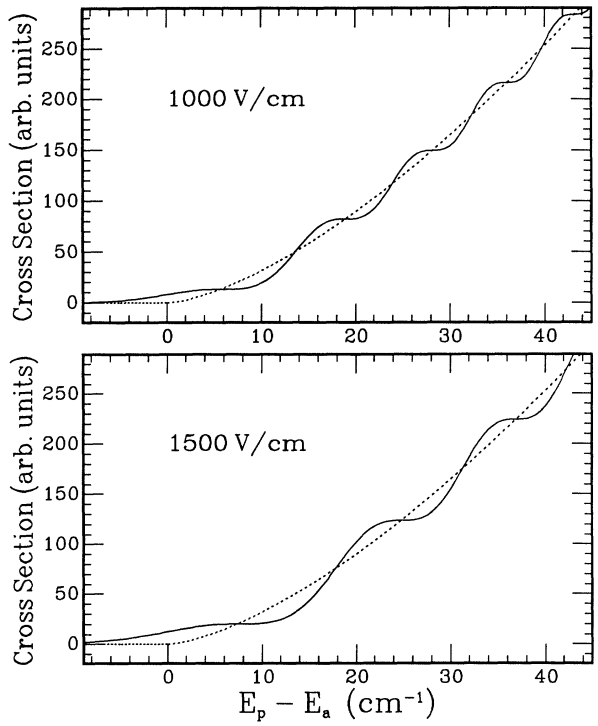

FIG. 1. p-wave Wigner law and field-on, parallel-case cross sections. The solid lines are the theoretical cross sections for photodetachment in electric fields parallel to the polarization direction and the dotted lines are the theoretical field-free cross sections. The cross sections are plotted in arbitrary units vs $E_p - E_a$, where E_p is the photon energy and E_a is the electron affinity.

$$\Psi_{k_x,k_y,\epsilon_z}(x,y,z)=\frac{\cos(k_x x)}{\sqrt{\pi}}\frac{\cos(k_y y)}{\sqrt{\pi}} \times\left[\frac{m}{2\hbar^2\epsilon_z}\right]^{1/4}\frac{i\sin(k_z z)}{\sqrt{\pi}} . \quad (14)$$

Combining Eqs. (2) and (14), and making use of Eq. (8), we obtain

$$|\langle f|\hat{\mathbf{e}}\cdot\mathbf{r}|i\rangle|^2=\left[\frac{D_0}{\pi}\right]^2\left[\frac{\beta}{\pi}\right]e^{-k_x^2/2\beta}e^{-k_y^2/2\beta} \times\left[\frac{m}{2\hbar^2\epsilon_z}\right]^{1/2} \times\left[\int_{-\infty}^{\infty}\frac{\sin(k_z z)}{\sqrt{\pi}}ze^{-\beta z^2}dz\right]^2 . \quad (15)$$

Now, unlike in the electric-field case, we can carry out the z integration analytically. By expanding the sine function in terms of exponentials and completing the square, we find

$$\int_{-\infty}^{\infty}\sin(k_z z)ze^{-\beta z^2}dz=\frac{k_z\sqrt{\pi}}{2\beta^{3/2}}e^{-k_z^2/4\beta} . \quad (16)$$

Using Eq. (16) in Eq. (15) and inserting the result into Eq. (1), we obtain

$$\sigma_{F=0}=4\pi^2\alpha E_p\int\left[\frac{D_0}{\pi}\right]^2\left[\frac{\beta}{\pi}\right]e^{-k_x^2/2\beta}e^{-k_y^2/2\beta}e^{-k_z^2/2\beta} \times\left[\frac{m}{2\hbar^2\epsilon_z\pi^2}\right]^{1/2}\frac{k_z^2\pi}{4\beta^3}dk_x dk_y d\epsilon_z \times\delta(E_p-E_a-E) . \quad (17)$$

Using the relationship $\epsilon_z=\hbar^2k_z^2/2m$, our previous definition of $E_\perp$, and changing variables, we get

$$\sigma_{F=0}=\pi^2\alpha E_p\left[\frac{D_0}{\pi}\right]^2\left[\frac{4m^2}{\hbar^4\beta^2}\right]\left[\frac{m}{2\hbar^2}\right]^{1/2} \times\int e^{-m(\epsilon_z+E_\perp)/\beta\hbar^2}\sqrt{\epsilon_z}dE_\perp d\epsilon_z \times\delta(E_p-E_a-E_\perp-\epsilon_z) . \quad (18)$$

Integrating over the δ function gives

$$\sigma_{F=0}=\pi^2\alpha E_p\left[\frac{D_0}{\pi}\right]^2\left[\frac{4m^2}{\hbar^4\beta^2}\right]\left[\frac{m}{2\hbar^2}\right]^{1/2} \times\int_0^{E_p-E_a}(E_p-E_a-E_\perp)^{1/2} \times e^{-m(E_p-E_a)/\beta\hbar^2}dE_\perp . \quad (19)$$

Integrating over $E_\perp$ gives the zero-field p-wave photodetachment cross section. In atomic units,

$$\sigma_{F=0}=\frac{8\alpha E_p D_0^2}{3\sqrt{2}\beta^2}(E_p-E_a)^{3/2}e^{-(E_p-E_a)/\beta} . \quad (20)$$

The dotted line in Fig. 1 shows the calculated cross section for zero-field p-wave photodetachment plotted in arbitrary units. Notice that $\sigma_{F=0}$ is zero at threshold ($E_p-E_a=0$), but σ_F is not. $\sigma_{F=0}$ is just the p-wave ($l=1$) case of the more general Wigner law [22],

$$\sigma_{\text{Wigner}}\propto(E_p-E_a)^{l+1/2} , \quad (21)$$

which can be obtained from similar arguments.

Above threshold, the photodetachment cross section in a static electric field can be expressed in terms of the cross section without the field and an oscillating function $H(E,F)$ which incorporates the effect of the field [6]. The unitless function $H(E,F)$ is defined as the ratio of the cross section in the field to the zero-field cross section. We write

$$\sigma_F=H(E,F)\sigma_{F=0} . \quad (22)$$

We can find the ratio of the cross section in the electric field to the zero-field cross section by dividing Eq. (13) by Eq. (20). We factor out the energy exponential and simplify the expression to

$$H(E,F)_{\text{par}} = \frac{3(2^{7/6})\beta^3}{F^{1/3}(E_p - E_a)^{3/2}} \times \int_{-\infty}^{E_p - E_a} d\epsilon_z e^{\epsilon_z/\beta} \times \left[\int_{-\infty}^{\infty} \text{Ai}(-\gamma) z e^{-\beta z^2} dz \right]^2 , \tag{23}$$

where the subscript "par" denotes the parallel polarization case. The limit as F goes to zero can be taken using the asymptotic expansion of the Airy function and in the limit $H(E,F)_{\text{par}}$ is equal to 1.0 as we would expect. We can write $H(E,F)_{\text{par}}$ in a more manageable form for numerical evaluation by explicitly using the long-wavelength condition specified earlier. When the wavelength of the final state is long, the variation of the Airy function is small over the width of the initial state. Hence we can Taylor expand the Airy function about the origin. In expanded form, the integral over z is trivial. The symmetry of the integrand is such that only the odd terms in the Airy expansion are nonzero. If we keep only the first nonzero term, we can write the spatial integral squared as

$$\left[\int_{-\infty}^{\infty} \text{Ai}(-\gamma) z e^{-\beta z^2} dz \right]^2 \cong \frac{\pi F^{2/3}}{2^{4/3}\beta^3} \left[\text{Ai}' \left[- \left[\frac{2}{F^2} \right]^{1/3} \epsilon_z \right] \right]^2 , \tag{24}$$

where the original z derivative has been modified via the chain rule so that the prime denotes the derivative with respect to $\epsilon_z(2/F^2)^{1/3}$. For the conditions we are interested in here, Eq. (24) is a very good approximation. Ten wave numbers above threshold, in a field of 1 kV/cm, and with a β value corresponding to a full-width-half-maximum radius of 1.3 Å, the second term in the expansion of the integral is 10^{-4} times the first term. The Taylor expansion used here serves essentially the same purpose as the δ-function approximation used in the s-wave theory [21]. Substituting Eq. (24) into Eq. (23) yields

$$H(E,F)_{\text{par}} \cong \frac{3\pi F^{1/3}}{2^{1/6}(E_p - E_a)^{3/2}} \times \int_{-\infty}^{E_p - E_a} e^{\epsilon_z/\beta} \times \left\{ \text{Ai}' \left[- \left[\frac{2}{F^2} \right]^{1/3} \epsilon_z \right] \right\}^2 d\epsilon_z . \tag{25}$$

Equation (25) will be our working equation for $H(E,F)_{\text{par}}$. Even with the approximation for the z integral, the ϵ_z integral is not analytic. Figure 2(a) shows $H(E,F)_{\text{par}}$ for three electric fields; the long-dashed line is for an electric field of 500 V/cm, the solid line is for 1000 V/cm, and the short-dashed line is for 1500 V/cm.

An interesting feature of the function $H(E,F)$ for both p wave and s wave [21] is that while the period of the oscillations is a function of the field, the amplitude is not. The height of each maximum is the same as the height of the corresponding maximum for other field values. The oscillations are simply more widely spaced at higher field values.

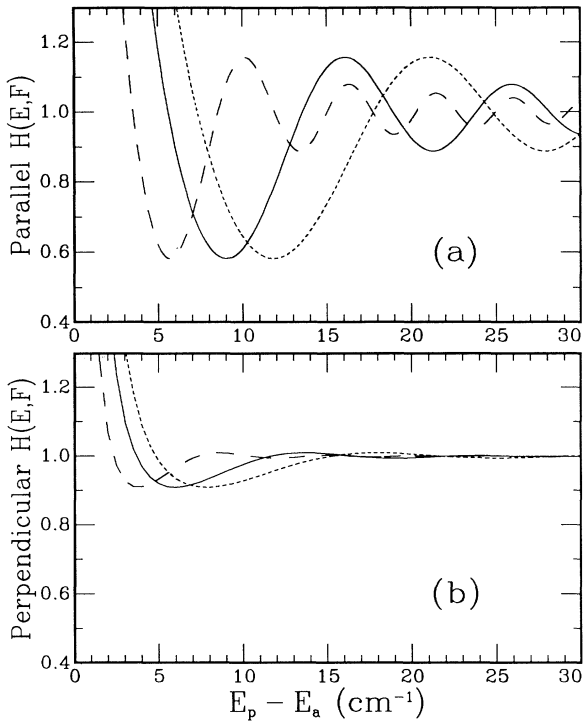

FIG. 2. (a) $H(E,F)_{\text{par}}$ for 500 V/cm (long-dashed line), 1000 V/cm (solid line), and 1500 V/cm (short-dashed line). (b) $H(E,F)_{\text{perp}}$ for 500 V/cm (long-dashed line), 1000 V/cm (solid line), and 1500 V/cm (short-dashed line).

We have not treated the binding potential of the negative ion in a detailed fashion. Although we have chosen a Gaussian to represent the initial state of the electron, that choice is not essential. In the present approximation, the only essential characteristic of the initial state is that it be short ranged. In the low-energy limit treated here, the large final-state wavelengths make it possible to neglect the details of the binding potential. It is therefore expected that any short-range initial state chosen should produce the same final results. Indeed, although we generally used a value for β corresponding to a full-width-half-maximum radius of 1 Å, the function $H(E,F)$ was verified to be independent of β over a range corresponding to widths of tenths to tens of angstroms. The insensitivity of $H(E,F)$ to the choice of β indicates that this model should be applicable to any negative ion bound in an s orbital as long as our original assumptions remain valid.

For detaching light polarized perpendicular to the electric-field direction, the detached electron travels out along p-wave lobes that are not along the field direction. The effects of the electric field should be less significant and we should expect smaller oscillations on the cross section. The calculation of $H(E,F)_{\text{perp}}$ is similar to the

calculation of $H(E,F)_{\rm par}$ and will therefore be presented in less detail.

We will use the same initial state here that we used for the parallel case [Eq. (2)]. The electric field will remain in the z direction and we will rotate the polarization direction ($\hat{\mathbf{e}}$) 90° so $\hat{\mathbf{e}}$ is in the x direction. In this case, the symmetry of the integrands is such that only the part of the final-state wave function that is odd in x and even in y will contribute. Equation (26) gives the contributing part of the final-state wave function.

$$\Psi_{k_x,k_y,\epsilon_z}(x,y,z)=\frac{i\sin(k_x x)}{\sqrt{\pi}}\frac{\cos(k_y y)}{\sqrt{\pi}}\times\left[\frac{4m^2}{e\hbar^4F}\right]^{1/6}\mathrm{Ai}(-\gamma)\ . \tag{26}$$

We will use Eq. (8) to perform the y integral and Eq. (16) to perform the x integral. The matrix element becomes

$$\langle f|\hat{\mathbf{e}}\cdot\mathbf{r}|i\rangle=\frac{D_0}{2\sqrt{\pi}}\left[\frac{4m^2}{e\hbar^4F}\right]^{1/6}e^{-(k_x^2+k_y^2)/4\beta}\frac{k_x}{\pi\beta^{1/2}}\times\int_{-\infty}^{\infty}\mathrm{Ai}(-\gamma)e^{-\beta z^2}dz\ . \tag{27}$$

Inserting Eq. (27) into Eq. (10) produces

$$\sigma_F=\frac{\alpha E_p D_0^2}{\pi\beta}\left[\frac{4m^2}{e\hbar^4F}\right]^{1/3}\times\int d\epsilon_z\int e^{-k_x^2/2\beta}k_x^2dk_x\times\int\left[\int_{-\infty}^{\infty}\mathrm{Ai}(-\gamma)e^{-\beta z^2}dz\right]^2\times e^{-k_y^2/2\beta}dk_y\,\delta(E_p-E_a-E)\ . \tag{28}$$

Now we will use $dk_i=(m/2\hbar^2E_i)^{1/2}dE_i$ and change variables. We were originally integrating over dk, from $-k_{\max}$ to $k_{\max}$. Since the k_x and the k_y integrands are even, we can rewrite the total integral as two times the integral from 0 to $k_{\max}$. This produces a factor of 2 for both the x and the y integrals. We can then change variables to E_x and E_y and Eq. (28) becomes

$$\sigma_F=\frac{\alpha E_p D_0^2}{\pi\beta}\left[\frac{4m^2}{e\hbar^4F}\right]^{1/3}\left[\frac{m^2}{\hbar^4}\right]4\int d\epsilon_z\int e^{-mE_y/\beta\hbar^2}\frac{1}{\sqrt{E_y}}dE_y\int\left[\int_{-\infty}^{\infty}\mathrm{Ai}(-\gamma)e^{-\beta z^2}dz\right]^2\sqrt{E_x}e^{-mE_x/\beta\hbar^2}dE_x\times\delta(E_p-E_a-E_x-E_y-\epsilon_z)\ . \tag{29}$$

Integrating over the δ function produces

$$\sigma_F=\frac{4\alpha E_p D_0^2}{\pi\beta}\left[\frac{4m^2}{e\hbar^4F}\right]^{1/3}\left[\frac{m^2}{\hbar^4}\right]e^{-(E_p-E_a)/\beta\hbar^2}\times\int_{-\infty}^{E_p-E_a}d\epsilon_z e^{m\epsilon_z/\beta\hbar^2}\int_0^{E_p-E_a-\epsilon_z}\frac{\sqrt{E_p-E_a-E_y-\epsilon_z}}{\sqrt{E_y}}dE_y\left[\int_{-\infty}^{\infty}\mathrm{Ai}(-\gamma)e^{-\beta z^2}dz\right]^2\ . \tag{30}$$

The integral over E_y is

$$\int_0^{E_p-E_a-\epsilon_z}\frac{\sqrt{E_p-E_a-E_y-\epsilon_z}}{\sqrt{E_y}}dE_y=\int_0^{E_p-E_a-\epsilon_z}\left[\frac{E_p-E_a-\epsilon_z}{E_y}-1\right]^{1/2}dE_y=\frac{\pi}{2}(E_p-E_a-\epsilon_z)\ . \tag{31}$$

Using the result of Eq. (31) in Eq. (30), we get

$$\sigma_F=\frac{4\alpha E_p D_0^2}{\pi\beta}\left[\frac{4m^2}{e\hbar^4F}\right]^{1/3}\left[\frac{m^2}{\hbar^4}\right]e^{-(E_p-E_a)/\beta\hbar^2}\times\int_{-\infty}^{E_p-E_a}d\epsilon_z\frac{\pi}{2}(E_p-E_a-\epsilon_z)e^{m\epsilon_z/\beta\hbar^2}\times\left[\int_{-\infty}^{\infty}\mathrm{Ai}(-\gamma)e^{-\beta z^2}dz\right]^2\ . \tag{32}$$

Simplifying Eq. (32) and converting to atomic units gives us the cross section for p-wave photodetachment in a perpendicular electric field,

$$\sigma_F=\frac{2^{5/3}\alpha E_p D_0^2}{\beta F^{1/3}}e^{-(E_p-E_a)/\beta}\times\int_{-\infty}^{E_p-E_a}d\epsilon_z(E_p-E_a-\epsilon_z)e^{\epsilon_z/\beta}\times\left[\int_{-\infty}^{\infty}\mathrm{Ai}(-\gamma)e^{-\beta z^2}dz\right]^2\ . \tag{33}$$

We can now use an approximation similar to the one we used to evaluate the z integral in the parallel case and plot the cross section. The solid line in Fig. 3 shows this cross section in 1000- and 1500-V/cm electric fields. The dotted line is the field-free cross section. Note that the scale is substantially changed from Fig. 1. The difference in the two cross sections is apparent only near the zero-

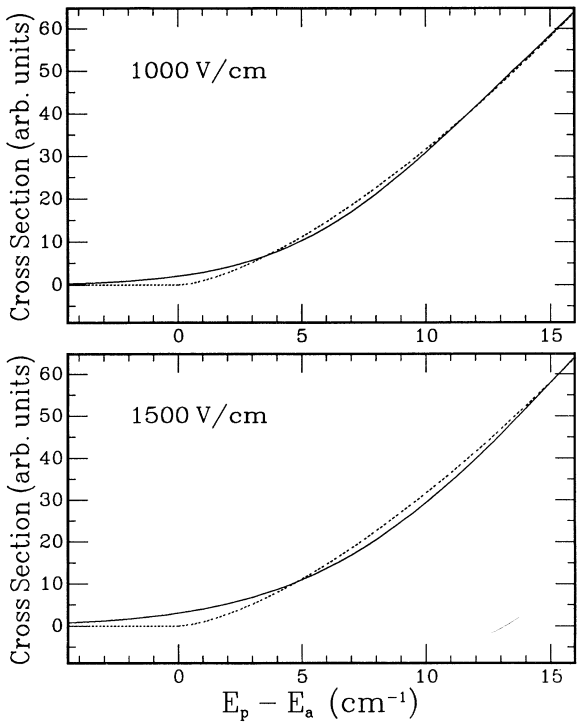

FIG. 3. p-wave Wigner law and field-on, perpendicular-case cross sections. The dotted line shows the zero-field p-wave photodetachment cross section and the solid line is the p-wave cross section for detachment in a perpendicular electric field. Note the scale change from Fig. 1.

field threshold. The difficulty in distinguishing the field-on and field-off cross sections demonstrates an advantage of using the ratio $H(E,F)$ to investigate field effects.

The zero-field cross section is the same as we calculated previously, so we will again use Eq. (20) in order to find the ratio of the field-on to the field-off cross section. The ratio of Eq. (33) to Eq. (20) is

$$H(E,F)_{\text{perp}} = \frac{3\beta}{2^{5/6}F^{1/3}(E_p-E_a)^{3/2}} \times \int_{-\infty}^{E_p-E_a} d\epsilon_z (E_p-E_a-\epsilon_z) e^{\epsilon_z/\beta} \times \left[\int_{-\infty}^{\infty} \text{Ai}(-\gamma) e^{-\beta z^2} dz\right]^2 . \tag{34}$$

In the limit as F goes to zero, the right-hand side of Eq. (34) is 1.0, as we would expect. We can again approximate the spatial integral over z by using a Taylor expansion. In this case only the even terms of the expansion produce nonzero terms, and we get

$$\left[\int_{-\infty}^{\infty} \text{Ai}(-\gamma) e^{-\beta z^2} dz\right]^2 \cong \frac{\pi}{\beta}\left[\text{Ai}\left[-\left[\frac{2}{F^2}\right]^{1/3}\epsilon_z\right]\right]^2 . \tag{35}$$

Substituting Eq. (35) into Eq. (34) gives us our working equation for $H(E,F)_{\text{perp}}$,

$$H(E,F)_{\text{perp}} \cong \frac{3\pi}{2^{5/6}F^{1/3}(E_p-E_a)^{3/2}} \times \int_{-\infty}^{E_p-E_a} (E_p-E_a-\epsilon_z) e^{\epsilon_z/\beta} \times \left\{\text{Ai}\left[-\left[\frac{2}{F^2}\right]^{1/3}\epsilon_z\right]\right\}^2 d\epsilon_z . \tag{36}$$

As in the parallel case, the integral over ϵ_z is not analytic.

Figure 2(b) shows $H(E,F)_{\text{perp}}$ for three electric-field values; the long-dashed line is for an electric field of 500 V/cm, the solid line is for 1000 V/cm, and the short-dashed line is for 1500 V/cm. The field dependence of the period of the oscillations is the same as in the parallel case. Figures 2(a) and 2(b) are both plotted with the same horizontal and vertical axes so that a comparison of the parallel and perpendicular field effects can be made easily. The difference in phase between the $H(E,F)_{\text{par}}$ and the $H(E,F)_{\text{perp}}$ oscillations results from the fact that $H(E,F)_{\text{par}}$ is the integral over the square of the first derivative of the Airy function and $H(E,F)_{\text{perp}}$ is the integral over the square of the Airy function.

Figure 4 compares the calculated $H(E,F)$ for 1000 V/cm for the two cases presented here to the s-wave calculation performed in our previous work [21]. The solid line is $H(E,F)$ for s-wave detachment, the long-dashed line is $H(E,F)_{\text{perp}}$, and the short-dashed line is $H(E,F)_{\text{par}}$. Detachment into an electric field perpendicular to the polarization direction has the smallest oscillations on the cross section, the spherically symmetric s-wave detachment has larger oscillations, and the p-wave detachment with the electric field parallel to the laser's

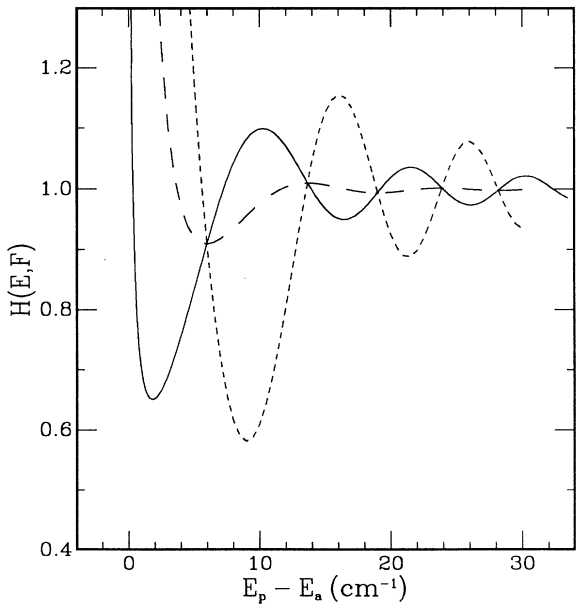

FIG. 4. $H(E,F)$ for 1000 V/cm for three cases, s wave (solid line), p-wave perpendicular case (long-dashed line), and p-wave parallel case (short-dashed line).

polarization direction shows the largest oscillations. The maximum oscillation height is determined by how much of the departing electron's wave packet travels along the electric field direction, since it is that part of the wave function which leads to interference. Note that near threshold the p-wave ratios are more strongly divergent than the s-wave ratio because of the slow rise of the field-free p-wave cross section.

III. EXPERIMENTAL APPARATUS

The experiments described in this paper were performed using a high-vacuum ion beam apparatus with a negative ion sputter source. A Nd:YAG (YAG denotes yttrium aluminum garnet) pumped pulsed dye-laser (PDL) beam was overlapped with the ion beam inside a set of parallel electric-field plates. The surviving ions were electrostatically deflected out of the beam and the neutral atoms were counted using a channeltron detector. The neutral counts were collected in 1-μs-wide bins using a computer-assisted data collection system. The basic apparatus is described in detail in Ref. [21]. The laser system and data analysis were somewhat modified; they are explained in further detail below.

The 537-nm light for the Au^- experiments was produced using Exciton Coumarin 540A (C540A) laser dye in methanol. About 1 W of 355-nm pump light was generated by sum-frequency mixing of the 1.064-μm Nd:YAG fundamental and the 532-nm second harmonic. The PDL was operated in the side-pumped mode and produced about 100 mW of laser power. The working concentrations for the laser dye were determined through trial and error. C540A needs to be about an order of magnitude more concentrated than many other dyes. An oscillator concentration of 1.20 g/l and an amplifier concentration of 275 mg/l were used [24]. The laser spot used for this experiment was apertured to remove low-power fringes and had a 1 mm by 3 mm cross section where it intersected the beam. The bandwidth of the 537-nm light should be slightly less than the 0.4 cm^{-1} measured for this laser in the red wavelength range since the fifth order of the PDL grating was used rather than the fourth order.

Above threshold, the data were collected in a manner which is relatively insensitive to temporal variations in the laser and ion beam intensities and in the overlap of the two beams. The laser fires every 50 ms and produces two trigger pulses: the q-switch pulse and a variable pulse. The variable pulse occurs before the q-switch pulse which marks the actual time the laser fires. The spacing can be moved 1–3 μs by adjusting a potentiometer on the laser head. Beginning with each variable q-switch pulse, the data were recorded in 32 1-μs-wide time bins. The variable pulse to q-switch pulse delay was adjusted so that the approximately 200-ns-wide Au^- detachment signal is contained entirely within one bin and the detachment signal from heavier ions falls in the next bin. Later bins are used to measure the neutral background due to collisional stripping so it can be subtracted out during the analysis. The data are taken with the electric field on during every other laser shot.

$H(E,F)$ is the ratio of photodetachment counts, not just the ratio of the number of counts in the signal bin. In order to measure $H(E,F)$, one needs three things: the total signal, the background signal, and the amount of photodetachment of other species of ions. The background is measured along with the signal for each laser shot since 32 1-μs bins are recorded. The average signal in each background bin is computed for each data file and these background signals are plotted separately for the field-on and field-off cases. Usually, some background structure can be seen. It is believed that the main sources of this structure are electrical laser noise, arrival of slower neutral atoms produced by photodissociation of molecules, electrons produced by the laser reflections striking objects inside the vacuum system, and photodetachment from negative ions with lower-energy thresholds than the ion being studied. Background bins are chosen separately for each data file in order to screen out these effects. The amount of detachment from more loosely bound ions is measured every 1–4 data points by tuning the laser far below threshold and measuring the signal with the same ion current and approximately the same laser power. Small changes in laser power do not seem to affect the below-threshold detachment signal. This signal is also largely independent of wavelength near the Au^- threshold, and is typically about 10% of the Au detachment signal. The field-on signal is then computed by taking the total number of counts in the field-on signal bin, subtracting the measured amount of below-threshold detachment, and then subtracting the average background. The same calculation is done for the field-off data and then the ratio $H(E,F)$ is determined by dividing the field-on signal by the field-off signal. Each data point represents 30–60 min of data collection time.

The ratio of detachment signal with the electric field on to that with the field off is measured as a function of laser photon energy and the result is directly compared with $H(E,F)$. While the ion beam current and the laser power vary on the time scale of minutes, the variations are very small over seconds and do not enter the data because the field is switched on and off every other laser pulse. The average detachment and standard deviation for all of the field-on data were computed as well as the average detachment signal and error for all of the field-off data. The ratio of these two values was then calculated and the error was computed by assuming that the errors in the field-on values and field-off values were uncorrelated. Further up on the cross section, where detachment signals are higher, this method yields ratios and errors very similar to those obtained by averaging the ratio from shorter time periods, as was done in the s-wave study [21].

IV. OBSERVATIONS

The p-wave photodetachment process is not spherically symmetric and therefore exhibits laser polarization dependence in an electric field. In the bound s-state to p-wave detachment case, the photodetached electron travels along the p-wave detachment lobes which are directed along the detaching laser's polarization direction. These

lobes have a $\cos^2\Theta$ shape. We have an axis externally defined by the static field direction so polarization-dependent effects can be investigated. In the case of an external electric field, this polarization dependence leads to a dramatic difference between detachment with the laser light polarized along the electric field and laser light polarized perpendicular to the electric-field direction.

We observe photodetachment in two different static electric fields, 1476(29) and 984(20) V/cm. The errors in the measurements of the applied field are due mostly to uncertainties in the electric-field plate spacing. The data will be presented grouped by polarization case, first with the light polarized parallel to the electric-field direction, and then with the light polarized perpendicular to the electric-field direction. The higher electric-field data are presented at the top of each graph. The ion velocity was parallel to the electric-field direction in both cases.

The ratio data obtained for Au^- in 1476- and 984-V/cm electric fields parallel to the light polarization are shown in Fig. 5 along with fits to the theoretical model. The zero-field Au^- detachment threshold does not appear on the graphs because the data range does not begin until roughly 5 cm^{-1} above threshold. Our detachment signal is too small to get meaningful ratio data closer to threshold.

The Au^- detachment curve in the 1476-V/cm parallel case was measured twice; the triangles in Fig. 5 represent data points from the full scan and the circles represent data points from the repeat scan. Unlike the multiple scans comprising the other data sets, the laser and the optics were completely realigned between these two data scans. Therefore it is possible that the angle between the laser beam and ion beam changed, giving rise to a different Doppler shift. Due to the velocity of the ion beam, there is a 0.11-cm^{-1} shift for each degree away from perpendicular. It is believed that any change in this shift is insignificant in this case. The solid line is a fit to $H(E,F)_{par}$ with both the field and the threshold as free parameters. The fit field value of 1478(12) V/cm for the 1476(29)-V/cm applied field shows remarkable agreement and, for both of the parallel data sets, the best fit was obtained with the threshold set to within 0.05 cm^{-1} of the accepted value [25]. The squares in Fig. 5 are the results

TABLE I. Summary of the experimental results.

Applied field (V/cm)	Fit field (V/cm)	Polarization direction
1476(29)	1478(12)	Parallel
984(20)	1044(8)	Parallel
1476(29)	1566(168)	Perpendicular
984(20)	1072(114)	Perpendicular

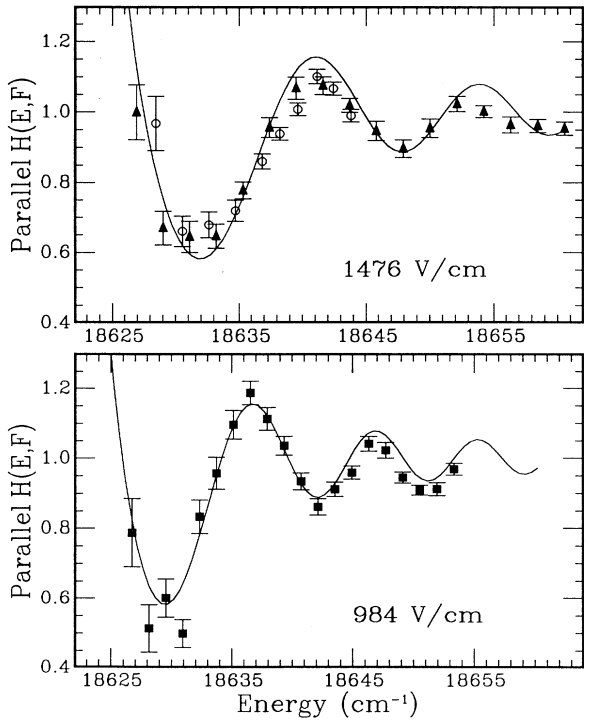

FIG. 5. Au^- photodetachment data with the electric-field direction parallel to the laser polarization. The field values on the figures are the applied fields. The values obtained from the fits are 1478(12) and 1044(8) V/cm. The laser was completely realigned between the data shown as open circles and the data shown as closed triangles in the 1476-V/cm graph.

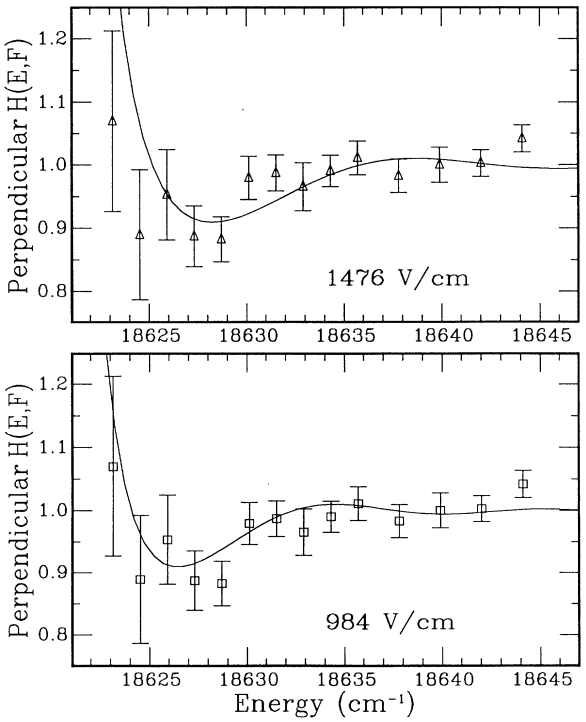

FIG. 6. Au^- photodetachment data with the electric-field direction perpendicular to the laser polarization. The field values on the figures are the applied fields. The values obtained from the fits are 1566(168) and 1072(114) V/cm.

for the photodetachment in a 984(20)-V/cm applied electric field. This data set fits to a field value of 1044(8) V/cm.

Figure 6 displays the data for photodetachment in a static electric field perpendicular to the laser polarization. Notice that both the horizontal and the vertical axes have changed between Figs. 5 and 6. As expected, the oscillations are greatly reduced for $H(E,F)_{\text{perp}}$. The error bars on the data points appear to be much larger than the perpendicular case for two reasons. Since some of the perpendicular-case data were taken nearer to threshold where the signal levels are lower, the statistical errors in these points are correspondingly higher. Additionally, the scale of the y axis has been expanded by almost a factor of 2 so the errors appear larger. The two fit field values of 1566(168) and 1072(114) V/cm are in good agreement with the applied fields. Table I summarizes the experimental results.

V. CONCLUSIONS

p-wave photodetachment from negative ions initially bound in s states has been studied in a static electric field. A simple theoretical prediction for the amplitude and the spacing of the oscillations has been presented. Oscillations on the p-wave cross section of Au^- were observed above threshold. The amplitude, phase, and periodicity of these oscillations have been compared to the model and are found to be in good agreement.

In these experiments, p-wave photodetachment has been studied by observing the ratio of field-on to field-off detachment. The strength of this technique is evidenced by the fact that we are able to measure perpendicular-case oscillations at the approximately 1-kV/cm fields used here. Harris *et al.* state that they are unable to see these oscillations for electric fields of less than about 1 MV/cm. In addition, unlike previous work, we studied electric-field effects on p-wave photodetachment from a nonhydrogenic ion. However, the model used does not take into account any of the nonhydrogenic effects. These data were taken for a different range of electric fields than the previous p-wave detachment data and the quality of the data permits a quantitative comparison with the theory. For the perpendicular case, the data agree with the model but this experiment is not a very sensitive test of the theory since the oscillatory structure is small. For the more dramatic oscillations of the parallel case, the ratio data taken here provide a more precise test of the theory than previous works. The data are found to be in good agreement with the model.

The agreement between the data and the model is in contrast to that observed in our recent experiments with s-wave detachment from S^- and Cl^- [21]. In those experiments, the measured amplitude of the oscillations on the cross section was consistently less (by about 20%) than that predicted by the model. Since both the s-wave and the p-wave studies were done with the same apparatus and techniques, it seems unlikely that the difference is an experimental artifact. In both the s-wave and p-wave cases, the model we use neglects any interaction between the electron and the neutral atom in the final state. Because of the short-range nature of the interaction, the effects, whether described as phase shifts [9,10] or rescattering [7], would be more significant for the s-wave detachment. Thus the s-wave and p-wave results, taken together, seem to support the possibility that the difference from the model observed in the s-wave data is due to the interaction of the detached electron with the neutral atom. Understanding whether or not that is the case requires further theoretical, and possibly experimental, investigation.

ACKNOWLEDGMENTS

The authors would like to thank C. W. Ingram for his helpful comments. This work was supported in part by the National Science Foundation.

[1] F. I. Dalidchik and V. Z. Slonim, Zh. Eksp. Teor. Fiz. **70**, 47 (1976) [Sov. Phys. JETP **43**, 25 (1976)].
[2] Yu. N. Demkov, V. D. Kondratovich, and V. N. Ostrovskii, Pis'ma Zh. Eksp. Teor. Fiz. **34**, 425 (1981) [JETP Lett. **34**, 403 (1981)].
[3] I. I. Fabrikant, Zh. Eksp. Teor. Fiz. **83**, 1675 (1982) [Sov. Phys. JETP **56**, 967 (1982)].
[4] W. P. Reinhardt, in *Atomic Excitations and Recombination in External Fields,* edited by M. H. Nayfeh and C. W. Clark (Gordon and Breach, New York, 1985).
[5] I. I. Fabrikant , Zh. Eksp. Teor. Fiz. **79**, 2070 (1980) [Sov. Phys. JETP **52**, 1045 (1980)].
[6] A. R. P. Rau and H.-Y. Wong, Phys. Rev. A **37**, 632 (1988).
[7] I. I. Fabrikant, Phys. Rev. A **40**, 2373 (1989).
[8] M. L. Du and J. B. Delos, Phys. Rev. A **38**, 5609 (1988).
[9] H.-Y. Wong, A. R. P. Rau, and C. H. Greene, Phys. Rev. A **37**, 2393 (1988).
[10] V. Z. Slonim and C. H. Greene, Radiat. Eff. Defects Solids **122/123**, 679 (1991).
[11] B. Gao and A. F. Starace, Phys. Rev. A **42**, 5580 (1990).
[12] H. C. Bryant, A. Mohagheghi, J. E. Stewart, J. B. Donahue, C. R. Quick, R. A. Reeder, V. Yuan, C. R. Hummer, W. W. Smith, S. Cohen, W. P. Reinhardt, and L. Overman, Phys. Rev. Lett. **58**, 2412 (1987).
[13] J. E. Stewart, H. C. Bryant, P. G. Harris, A. H. Mohagheghi, J. B. Donahue, C. R. Quick, R. A. Reeder, V. Yuan, C. R. Hummer, W. W. Smith, and S. Cohen, Phys. Rev. A **38**, 5628 (1988).
[14] P. G. Harris, H. C. Bryant, A. H. Mohagheghi, C. Tang, J. B. Donahue, C. R. Quick, R. A. Reeder, S. Cohen, W. W. Smith, J. E. Stewart, and C. Johnstone, Phys. Rev. A **41**, 5968 (1990).
[15] P. Frey, F. Breyer, and H. Hotop, J. Phys. B **11**, L589 (1978).
[16] P. Frey, M. Lawen, F. Breyer, H. Klar, and H. Hotop, Z. Phys. A **304**, 155 (1982); **306**, 185(E) (1982).
[17] C. H. Greene and N. Rouze, Z. Phys. D **9**, 219 (1988).
[18] M. C. Baruch, T. F. Gallagher, and D. J. Larson, Phys. Rev. Lett. **65**, 1336 (1990).

[19] M. C. Baruch, W. G. Sturrus, N. D. Gibson, and D. J. Larson, Phys. Rev. A **45**, 2825 (1992).
[20] L. A. Bloomfield, Phys. Rev. Lett. **63**, 1578 (1989).
[21] N. D. Gibson, B. J. Davies, and D. J. Larson, Phys. Rev. A **47**, 1946 (1993).
[22] E. P. Wigner, Phys. Rev. **73**, 1002 (1948).
[23] L. D. Landau and E. M. Lifshitz, *Quantum Mechanics* (Pergamon, New York, 1977), p. 74.
[24] Amplifier dye breakdown was a problem with the uv pumping. The addition of approximately 1.0 g/liter of a compound known as DABCO (diazabicyclo-octane, from Aldrich Chemical Company, Inc.) was used to extend the amplifer dye life to about 12 h. The lifetime of the dye without DABCO was not investigated since a quick test showed that its addition did not lower the laser power or shift the power curve. See R. von Treba and T. H. Kock, Chem. Phys. Lett. **93**, 315 (1982).
[25] H. Hotop and W. C. Lineberger, J. Chem. Phys. **58**, 2379 (1973).